Correlation between hole insertion criteria in a boundary element and level set based topology optimisation method

B.Ullah*, J.Trevelyan

School of Engineering and Computing Sciences, Durham University,
South Road, Durham DH1 3LE, UK.

Abstract

The research work presented in this paper is based on the correlation between two hole insertion criteria in a boundary element method (BEM) and level set method (LSM) based structural topology optimisation scheme for 2D elastic problems. The hole insertion criteria used in this work are based on the von Mises stress and the topological derivative approaches. During the optimisation process holes are automatically inserted in the design domain using each of the two criteria. The LSM is used to provide an implicit description of the structural geometry, and is also capable of automatically handling topological changes, i.e. holes merging with each other or with the boundary. The evolving structural geometry (i.e. the zero level set contours) is represented by NURBS, providing a smooth geometry throughout the optimisation process and completely eliminate jagged edges. In addition the optimal NURBS geometry can be used directly in other design processes.

---

*Corresponding author

Email addresses: `baseer.ullah@durham.ac.uk` (B.Ullah),
`jon.trevelyan@durham.ac.uk` (J.Trevelyan)

Four different benchmark examples are considered in this study and each is tested against the two hole insertion criteria. The results obtained validate the proposed optimisation method and we demonstrate a clear correlation between the two hole insertion criteria.

1. Introduction

Structural optimisation is a very active field of research. There are various methods and techniques available for size, shape and, the most challenging and versatile, i.e. topology optimisation problems, but the development of new efficient topology optimisation methods remains an active research area. Some of the methods developed for structural optimisation are based on the LSM presented by Osher and Sethian [1], which has emerged as a powerful tool for describing the evolution of structural boundaries in an optimisation process. The first application of LSM for topology optimisation was presented by Sethian and Wiegmann [2]. In the case of 2D structural optimisation, the LSM is unable on its own to nucleate holes during the optimisation process. Therefore, in the early research work carried out, the optimisation techniques were dependent on the use of an initially guessed topology ([3, 4]). Allaire and Jouve [5] combined the shape derivatives with topological derivatives to present a level set based optimisation method capable of automatic hole insertion. Other examples of LSM-based structural optimisation schemes can be found in [6, 7, 8, 9, 10, 11].

In most of the above optimisation techniques, the structural analysis was carried out with the finite element method (FEM). Each optimisation iteration modifies the structural geometry, and as a result the standard FEM requires re-meshing, usually of the complete design domain, incurring a high computational cost. The requirement of a smooth optimal geometry further increases the computational cost due to mesh refinement at the boundaries. To reduce the computational cost, a fixed grid type approach can be utilized as an alternative FE analysis tool [3, 4, 5, 6, 8, 9, 10]. Allaire *et al.* [4] used a simple "ersatz material" approach in which holes of the structure are replaced by a specified minimum relative density and the boundary element stiffness is assumed to be proportional to the structural material within the element. although this is a simple approach, but is not effective to capture the exact geometry of the boundary [4] and the only way to obtain an accurate solution near the boundary a highly dense grid distribution is required [12]. Furthermore, the smoother structural boundaries can be obtained by adding a small term to the boundary velocity proportional to the curvature of the shape [4]. A smoothed Heaviside function approach [3, 8, 9] is adopted to smooth the discontinuity at the boundary. However, the numerical integration of the stiffness matrix may be less accurate [13]. Wei *et al.* [14] used a fixed grid X-FEM approach for an LSM based topology optimisation. In addition, there are a few FEM based level set methods which uses some form of re-meshing strategies during the optimisation iterations, e.g. [13, 15, 16]. The BEM [17] is a well-established alternative to the FEM in structural analysis, and is attractive because it requires discretisation only at the structural boundary. This reduction of problem dimensionality considerably simplifies

3

the re-meshing task, which can be performed efficiently and robustly. Furthermore, the BEM requires boundary element on the level set boundary and avoids approximation at the boundary, which is the case for the fixed grid type approaches usually employed. Thus, its rapid and robust re-meshing and accurate boundary stress solutions make the BEM a natural choice in the field of shape and topology optimisation.

Cervera and Trevelyan [18, 19] used BEM for structural optimisation of two and three dimensional problems. The developed algorithm creates internal holes during the optimisation process based on the von Mises stress. Additional care was taken to handle hole merging during the optimisation process. The boundary element based topological derivatives concept was used by Marczak [20] and Cisilino [21] for the topology optimisation of potential problems. The derivation of the topological derivative formulation in these methods was based on the work of Novotny *et al.* [22], who presented a new computational approach of the topological sensitivity analysis. Carretero and Cisilino [23] presented topology optimisation of 2D elastic structures using BEM. In their work, the topological derivative obtained, uses the total potential energy as a cost function. The topological derivative approach was further combined with a hard kill material removal scheme by Marczak [24] for the optimisation of 2D elastic structures in a BEM framework. In the above discussed methods an additional mechanism is always required to handle topological changes, i.e. holes merging with each other or with the boundary during the optimisation iterations. In addition, the evolving geometry and the final optimal in [23] and [24] also exhibit jagged edges.

The use of BEM with the level set method in structural optimisation was first considered by Abe *et al.* [25]. A design sensitivity analysis was used as a criterion to update the structural geometry during the optimisation process. The use of sensitivity analysis prohibits this method from nucleating new holes, and makes this method highly dependent on the initially guessed topology. Yamasaki *et al.* [26] presented an immersed boundary element method for structural optimisation, which is also dependent on the initially guessed topology.

Most level set topology optimization methods are gradient based (through the use of shape sensitivities). These techniques are popular because they are efficient although it requires computation of suitably accurate gradients, which may not be available. Moreover, these methods can often have difficulties in dealing with local optima, they are complex algorithms that are difficult to implement efficiently and with noise generated when small changes in the design variables cause changes in topology. In general, the algorithms are well established, e.g., [3, 4, 5, 6]. Compared to their gradient-based counterparts, the evolutionary optimisation methods have advantages such as global optimum searching ability and parallel computing [7]. These methods are simple to use, robust, and capable of dealing with almost any kind of structural optimisation problem, for example, ESO [27]. There has been some controversy over the last decade over the validity of ESO as an optimisation approach when the removal and addition of material is provoked by local stress values, in contrast with the use of design sensitivities related to an objective function. In spite of this, ESO schemes have remained popular on account of their simplicity and extensive empirical evidence of the fact

that their optimal solutions closely resemble those derived by more rigorous descent methods (e.g. Li *et al.* [28]).

The combination of LSM and BEM requires a comprehensive investigation to effectively utilize their attractive properties in the field of structural optimisation. Works in combined BEM and LSM to date appear computationally expensive. A new optimisation method is proposed in this paper which overcomes the deficiencies in the above methods. This new approach is based on the BEM and LSM with an evolutionary optimisation technique. The proposed method automatically inserts holes during the optimisation process. The criteria for hole insertion may be based on two different approaches, i.e. von Mises stress and topological derivative [22, 23]. This research work also discusses, in detail, the correlation between the two different criteria with the help of some numerical tests. After the hole insertion a shape optimisation procedure is carried out, which either adds or removes material with outward or inward boundary movements, based on the von Mises stress at the structural boundaries.

In the BEM and topological derivative based methods ([23, 24]), the structural geometry also suffers from jagged edges throughout the optimisation process. The use of these jagged edges in an optimisation process create artificial stress concentration regions in the structure, which can mislead the optimisation process. The occurrence of these artificial stress concentration regions can be avoided with the use of a fine BEM mesh, but at the same time this will increase the computational cost of the optimisation process. In order to overcome this problem, an alternative approach has been proposed in this paper. During the optimisation process, at the end of each

optimisation iteration after the update of level set function, a NURBS fitting procedure fits smooth curves through the zero level sets. This procedure provides a modified geometry in a standard CAD representation, which not only overcomes the jagged edge issue but at the same time the final optimal geometry can be directly used in other design processes.

The proposed method uses the 2D version of the BEM analysis software Concept Analyst **(CA)** [29]. The remainder of this paper is organised as follows. The basic details of LSM are introduced in Section 2, the BEM is developed in Section 3. In Section 4 we present the details of the optimisation algorithm and its implementation. The results obtained from the proposed algorithm are presented and discussed in Section 5, and the paper closes with some concluding remarks in Section 6.

2. Level set method

The LSM is an efficient numerical technique developed by Osher and Sethian [1] for the tracking of propagating interfaces. There is a wide variety of applications, including structural optimisation, in which LSM is successfully implemented. The propagation of the structural boundary during optimisation iterations can be linked with the evolution of a function ϕ as an initial value problem. This means that the position of the structure boundary at any time t is given by the zero level set of the function ϕ. The evolution equation of the LSM given in [1] is

$$\frac{\partial \phi}{\partial t} + F|\nabla \phi| = 0 \tag{1}$$

where F is the velocity in the normal direction and t is the virtual time.

In the implicit representation the connectivity of the discretisation does not need to be determined explicitly. This is one of the most interesting features of the implicit geometric representation, in that merging and breaking of curves in 2D and surfaces in 3D can be handled automatically. The implicit method uses the Eulerian approach to represent an evolving geometry. We define Ω^- as the region contained within the boundary, Ω^+ as the union of the regions inside holes and the region of the design domain outside the boundary, and the contour $\partial\Omega$ as the interface between the non-overlapping regions Ω^- and Ω^+. These definitions are expressed as follows and shown in Figure 1.

$$\phi(\vec{x}) \begin{cases} < 0 & \vec{x} \in \Omega^- \\ = 0 & \vec{x} \in \partial\Omega \\ > 0 & \vec{x} \in \Omega^+ \end{cases} \tag{2}$$
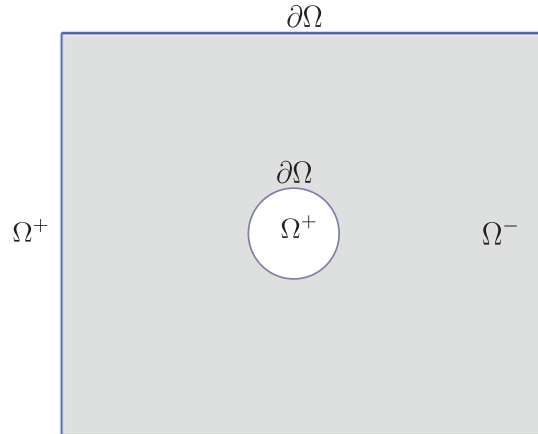

Figure 1: Geometry implicit representation

3. Boundary element method

The Boundary Element Method (BEM) is a standard technique for computational solution of partial differential equations. There are numerous textbooks describing the method (e.g. Becker [17]), but for completeness a brief description is included in this section.

We consider linear elasticity in the domain $\Omega^- \subset \mathbb{R}^2$, having boundary $\partial\Omega = \Gamma$. The boundary includes an exterior boundary and may contain interior boundaries to model holes in the structure. These will be important as design topologies develop. We solve the equilibrium equations

$$\sigma_{ij,j}(\vec{x}) + b_i(\vec{x}) = 0, \qquad \vec{x} \in \Omega^- \tag{3}$$

where $i, j = x, y$, the problem being subject to boundary conditions

$$u_i(\vec{x}) = \bar{u}, \qquad \vec{x} \in \Gamma_u \tag{4}$$

$$t_i(\vec{x}) = \bar{t}, \qquad \vec{x} \in \Gamma_t \tag{5}$$

In the above, u_i represents a displacement component, σ the Cauchy stress tensor and b the body force vector. We define $\Gamma = \Gamma_u \cup \Gamma_t$, but since it is commonplace in practice to prescribe different boundary condition types in different coordinate directions at the same point, this definition is purely symbolic. The traction component, t_i, is given by

$$t_i(\vec{x}) = \sigma_{ij}(\vec{x})n_j(\vec{x}), \qquad \vec{x} \in \Gamma \tag{6}$$

where n is the unit outward pointing normal vector at $\vec{x}$. The terms $\bar{u}, \bar{t}$ are prescribed known displacements and tractions respectively. The Einstein summation convention is assumed throughout. Taking for simplicity here

the case $b = 0$, the differential equations (3) can be transformed into an equivalent integral equation form known as the Somigliana identity. We may write

$$c_{ij}(\vec{x})u_j(\vec{x}) + \fint_\Gamma T_{ij}(\vec{x}, \vec{y})u_j(\vec{y})d\Gamma(\vec{y}) = \int_\Gamma U_{ij}(\vec{x}, \vec{y})t_j(\vec{y})d\Gamma(\vec{y}) \qquad (7)$$

where T_{ij}, U_{ij} are respectively the traction and displacement kernels, or fundamental solutions. The free coefficients, c_{ij}, arise from the strong singularity in the integral containing the traction kernel; this integral is denoted $\fint$ to indicate its evaluation in the Cauchy Principal Value sense. The boundary may be discretised using elements, i.e.

$$\Gamma = \bigcup_{e=1}^{N_e} \Gamma_e, \qquad \Gamma_i \cap \Gamma_j = \emptyset, i \neq j \qquad (8)$$

and the geometry of each element parameterised in terms of a local intrinsic coordinate $\xi^e \in [-1, 1], e = 1, ..., N_e$, allowing (7) to be rewritten

$$c_{ij}(\vec{x})u_j(\vec{x}) + \sum_{e=1}^{N_e} \sum_{l=1}^{m} \left[\int_{-1}^{+1} T_{ij}(\vec{x}, \vec{y}(\xi^e))N_l(\xi^e)J^e(\xi^e)\,d\xi^e \right] u_j^{el}$$

$$= \sum_{e=1}^{N_e} \sum_{l=1}^{m} \left[\int_{-1}^{+1} U_{ij}(\vec{x}, \vec{y}(\xi^e))N_l(\xi^e)J^e(\xi^e)\,d\xi^e \right] t_j^{el} \qquad (9)$$

where l is a local node number, on element e, that varies from 1 to $m = 2, 3, ...$ for linear, quadratic elements etc., $\vec{y}$ is the location on the element corresponding to the variable of integration ξ^e, N_l is the Lagrangian shape function for node l, $J^e = d\Gamma_e/d\xi^e$ is the Jacobian of transformation and u_j^{el} and t_j^{el} are displacements and tractions, respectively, at local node l on element e. Taking point $\vec{x}$ to be a node point, and evaluating the boundary integrals in (9) using a suitable scheme that copes with the singularities in

the fundamental solutions, we arrive at

$$c_{ij}(\vec{x})u_j(\vec{x}) + \sum_{e=1}^{N_e}\sum_{l=1}^{m} h^{el}u_j^{el} = \sum_{e=1}^{N_e}\sum_{l=1}^{m} g^{el}t_j^{el} \tag{10}$$

where h^{el}, g^{el} are the evaluated integrals. Finally, placing point $\vec{x}$ at each node in turn, equations of this form may be developed at each, and these may be assembled to form a linear system

$$[\mathbf{H}]\{\mathbf{u}\} = [\mathbf{G}]\{\mathbf{t}\} \tag{11}$$

where the matrices $\mathbf{H}$ and $\mathbf{G}$ contain the coefficients h^{el} and g^{el} respectively, and multiply vectors of nodal displacements and tractions. Application of the boundary conditions (4) and (5) reduces the problem to a square system that can be solved for unknown boundary displacements and tractions.

It is important in topology optimisation to determine accurate solutions at *internal points*, i.e. points $\vec{x} \in \Omega^-\backslash\Gamma$. Once equation (11) has been solved, internal point displacements can be found using (9) by taking $\vec{x}$ as the point in question and letting $c_{ij} = \delta_{ij}$, where δ_{ij} is the Kronecker delta, and likewise stress components may be determined from a differentiated form of the same expression.

4. Optimisation algorithm

The idea to enhance the performance of a structure based on providing maximum possible stiffness against the applied loads is the basis of the maximum stiffness criterion. However, simply seeking to maximise stiffness will lead to an increase in the weight of the structure, because the design space will become completely filled with material. In order to enhance the

11

structural performance from both the stiffness and efficient material utilization points of view the concept of specific stiffness was developed [30], being defined as,

$$f_K = \frac{K}{V} \tag{12}$$

where K is the stiffness and V is the volume of the structure. An equivalent concept in terms of the compliance is the specific strain energy, f_U, which is the product of strain energy U and the volume V of the structure [18], i.e.

$$f_U = UV \tag{13}$$

The expression used for strain energy calculation is,

$$U = \int_\Gamma \frac{1}{2} t_i u_i d\Gamma \tag{14}$$

In practice, since the product $t_i u_i$ is non-zero only over elements on which a non zero traction boundary condition has been prescribed (assuming there are no non-zero displacement constraints applied) the integral involved in Equation (14) conveniently reduces to the integral taken only over these elements.

The optimisation progress can be monitored using the reduction in f_U, and the target volume fraction can be used as a stopping criterion. The volume fraction α at a given stage of optimisation process can be defined as,

$$\alpha = V/V_0 \tag{15}$$

where V is the volume at the current iteration (this is interpreted as the area in a 2D representation) and V_0 the initial volume of the structure.

The main steps in this optimisation process are summarised as follows:

1. Define structural geometry with applied loads and constraints.

2. Initialize level set grid with signed distance function.

3. Carry out boundary element analysis.

4. Insert holes in the structure based on the chosen hole insertion criterion.

5. Identify high and low stress boundary nodes based on the material addition and removal criterion, and assign positive velocity values to high stress boundary nodes, while negative velocity values to the low stress boundary nodes.

6. Solve the level set equation based on the velocity values assigned in step 5 to evolve the topology of the structure.

7. Trace the zero level set contours and convert them into a standard CAD representation, i.e. NURBS.

8. Repeat the above procedure from step 3, until the stopping criterion is satisfied.

The implementation of the above optimisation algorithm is shown in Figure 2 and discussed in the following sections in detail. Many of these steps involve criteria of various types involving the comparison of stresses, volumes, etc., against various coefficients. These have been developed through extensive numerical testing on a range of optimisation problems.

4.1. Structure geometry, loading and constraints

In the first step of this optimisation method loading and constraints are applied to a given structure which needs to be optimised. The geometry of this initial structure is arbitrary, and is defined as a polygon in which each edge is a line segment which may be straight or curved. In most research
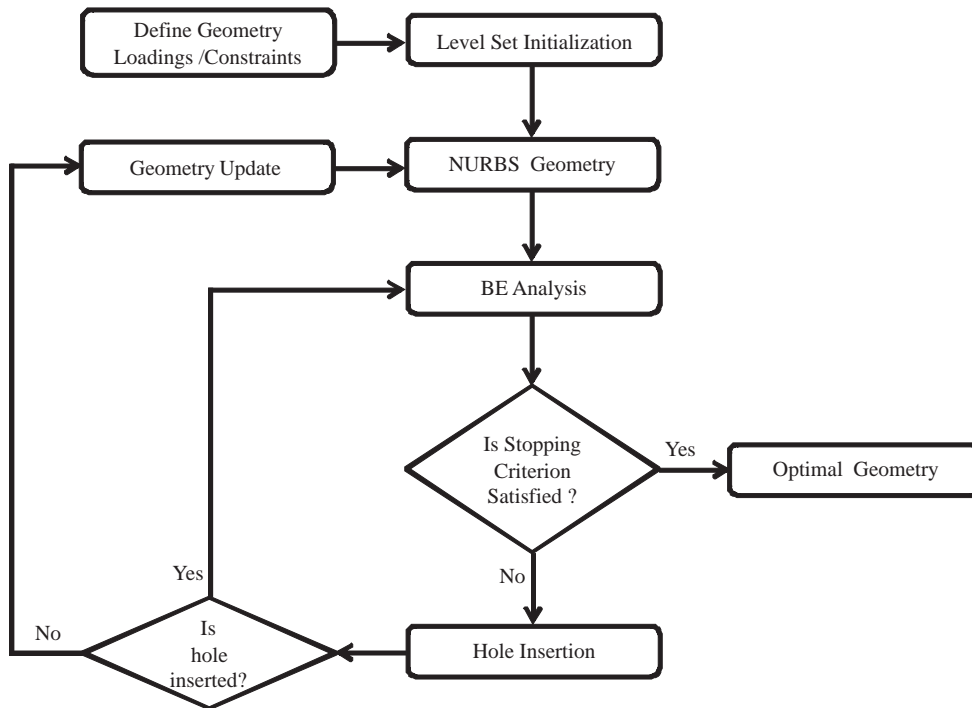
Figure 2: Optimisation flow chart

work of this type, the initial geometry is a simple rectangle. For explanation of various portions of the structural geometry, the example of a cantilever beam is shown in Figure 3. The line segments describing portions of the boundary over which loads (right edge) and constraints (top and bottom of left edge) are prescribed, highlighted as dark lines in Figure 3, remain fixed, while the remaining line segments are allowed to be modified during the optimisation process. The modifiable line segments shown in Figure 3a are first converted into NURBS (Figure 3b) prior to the BEM structural analysis. The conversion details of line segments into NURBS are explained in Section 4.4. In this particular example there are three NURBS segments shown in Figure 3b.

14

(a) Initial geometry   (b) NURBS geometry
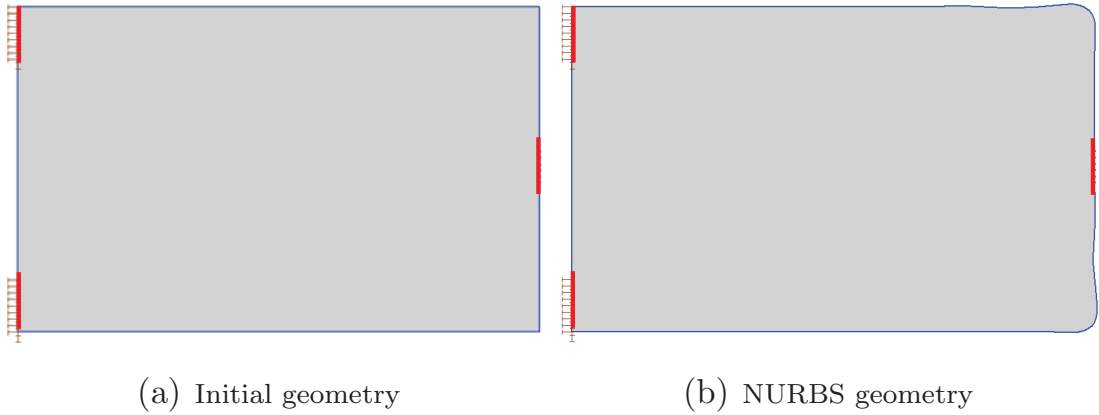
Figure 3: Defining structural geometry

4.2. Geometry update

In this new approach of LSM based structural optimisation, the geometric update is carried out in a two step procedure. In the first step holes are inserted in the design domain based on the hole insertion criteria discussed in the following subsection, which is then followed by a shape optimisation step. In the shape optimisation step, a bi-directional evolutionary approach is used to add and remove material through structural boundary movements, either outward or inward, based on the von Mises stress criterion.

4.2.1. Criteria for hole insertion

This section discusses the hole insertion criteria, their correlation and the implementation details. In a BEM analysis stresses (or any other required property) within the design domain are calculated at internal points. These results are then used to guide hole insertion at the desired location. The CA software generates these points automatically and then calculates any required property at these points. It should be noted that the procedure for

defining the internal point locations includes some randomness, and this can lead to a minor asymmetry in some design geometries as the optimisation progresses.

Criterion A

The first hole insertion criterion is based on the removal of material around the internal points with the lowest value of von Mises stress (σ_V). Li *et al.* [28] showed that the criterion of von Misses stress in the classical evolutionary structural optimisation (ESO) method is equivalent to the compliance minimisation criterion. Furthermore, it is suggested that the compliance minimisation problem can be solved by directly using the von Mises stress criterion, and vice versa. Therefore no significant conflict in using a stress criterion alongside strain energy based performance indicator. We present the definition of σ_V, as

$$\sigma_V = \frac{1}{\sqrt{2}}\sqrt{(\sigma_1 - \sigma_2)^2 + (\sigma_2 - \sigma_3)^2 + (\sigma_3 - \sigma_1)^2} \tag{16}$$

where σ_1, σ_2 and σ_3 are the principal stresses. Based on this criterion, holes are inserted around the internal points which satisfy the following conditions.

$$\sigma_V(i) \leq (1 + k_V)\, \sigma_{Vmin} \tag{17}$$

where $\sigma_V(i)$ is the von Mises stress at a given internal point i, σ_{Vmin} is the minimum value of von Mises stress over all internal points in the current iteration and k_V is the von Mises stress threshold factor. The value of σ_{Vmin} needs to be modified a little, since it is quite common for an internal point to be located in a region of very low σ_V (on the neutral axis in a bending problem, for example). Instead of using the minimum value, we use the

average of the five smallest values of σ_V. The material removal during the optimisation process is also dependent on the value of k_V. If k_V is chosen to be very small the creation of holes is inhibited, whereas a large k_V will give rise to the insertion of very large holes which destabilises the process. Based on the numerical tests conducted k_V should be used with values in range $0.3 \leq k_V \leq 0.6$. For simplicity we can write $(1 + k_V)$ as f_V. The complete details of the hole insertion procedure are discussed in Section 4.2.2.

Criterion B

The second criterion is based on a sensitivity analysis, i.e. the topological derivative concept. The original concept of topological derivative is related to the sensitivity of a cost function when material is removed from the design domain through a small hole insertion. However, the difficulty of establishing a direct mapping between the two different domains (i.e. the domain with and without a hole) restricts its implementation in an optimisation problem. Novotny *et al.* [22] presented an alternative approach to overcome the difficulty associated with the original definition. Based on this new approach, a hole creation is equivalent to the idea of perturbing a pre-existing hole, whose radius tends to zero. Thereby providing the possibility to establish a direct mapping between the initial and modified domains. This idea has been used for the derivation of the most useful and easy to implement formulation of the topological derivative (for details see [22]). In a BEM framework this concept has been used by Carretero and Cisilino [23], and Marczak [24], for the optimisation of 2D elasticity problems with the total strain energy as the cost function. In their work the topological derivative $D_T(\vec{x})$ used was a

function of the stress invariants, i.e.

$$D_T(\vec{x}) = \frac{2}{1+\nu}\,\sigma \cdot \epsilon + \frac{3\nu - 1}{2(1-\nu^2)}\,tr\sigma tr\epsilon \tag{18}$$

where $tr\sigma$ and $tr\varepsilon$ represent the trace of the stress and strain tensors, respectively. According to this criterion, holes are inserted in the design domain around the internal points satisfying the following conditions.

$$D_T(i) \leq (1 + k_T)\,D_{Tmin} \tag{19}$$

where $D_T(i)$ is the topological derivative at a given internal point i, D_{Tmin} is the minimum value of topological derivative over all internal points in the current iteration and k_T is the topological derivative threshold factor. Similar to factor k_V, the size of the inserted hole is also dependent on the value of k_T. The selection of k_T is based on a correlation found between the two hole insertion criteria (discussed in detail in the following section) and is related to k_V. For simplicity we can write $(1 + k_T)$ as f_T. The hole insertion implementation details are discussed in Section 4.2.2.

Correlation between Criterion A and B

It can be seen that the expressions of σ_V (16) and topological derivative (18), are based on the stress invariants; this suggests a possible correlation between criteria A and B. In order to deduce this correlation we consider the results obtained for the calculation of σ_V and D_T for various stress states in a plane stress condition, i.e. $\sigma_1, \sigma_2 \in [0; 50], \sigma_3 = 0$. Figures 4a and 4b show plots of σ_V and ${\sigma_V}^2$ against D_T, respectively. It is evident from this comparison, that an approximately linear relationship exists between ${\sigma_V}^2$ and D_T. Similarly, using the set of points previously selected, some contour

plots are generated for $(\sigma_V/\sigma_{Vmax})^2$ and (D_T/D_{Tmax}) (shown in Figures 5a and 5b, respectively), which show this correlation between the two criteria in another form. It is evident that the two approaches are strongly correlated
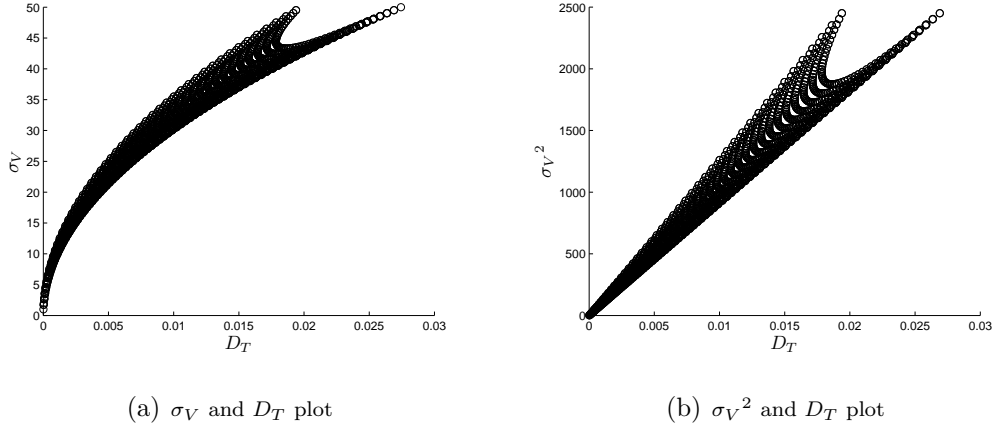

(a) σ_V and D_T plot

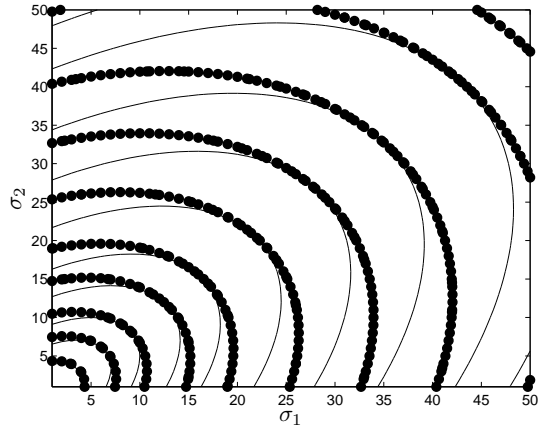(b) $\sigma_V{}^2$ and D_T plot

Figure 4: Correlation between σ_V and D_T

Figure 5: $(\sigma_V/\sigma_{Vmax})^2$ and (D_T/D_{Tmax}) contours (-,•)

when $\sigma_1 \approx \sigma_2$, suggesting a relationship

$$D_T(i) \;\approx\; C\sigma_V{}^2(i) \qquad\qquad (20)$$

where C is a constant whose value is a function of the material properties. When σ_1 and σ_2 are very different, the behaviour still appears to corresponds to (20) but with a different constant C. This behaviour is also evident from the straight lines bonding the point distribution in Figure 4b. To proceed with an investigation into the correlation between the two criteria, we will assume a quadratic relationship

$$D_T(i) \;=\; C\sigma_V{}^2(i) \qquad\qquad (21)$$

which implies a relation between hole insertion factors

$$f_T \;=\; f_V{}^2 \qquad\qquad (22)$$

All examples presented in this paper will have factors (f_T and f_V) chosen in accordance with this relation.

4.2.2. Hole insertion

The main steps followed for hole insertion based on the two criteria are explained in Table 1 and for clarity also shown in Figure 6.

The hole insertion changes the structural geometry, which is re-analyzed with BEM for the new stress distribution.

4.2.3. Shape optimisation

In this step of the optimisation process, only the existing structural boundaries are modified. The boundary modification approach is based on

	Criterion A	Criterion B
1	Sort all the internal points in ascending σ_V order.	Sort all the internal points in ascending $D_T(\vec{x})$ order.
2	Identify internal points satisfying (17)	Identify internal points satisfying (19)
3	The first internal point from step 1 is used as a centre, depicted with ▲ in Figure 6b, for the new hole. Similarly points identified in step 2 are depicted with ■ in Figure 6b. If fewer than five such points are identified, abort the hole insertion	
4	Internal points satisfying a threshold stress level around the central point from step 2, are used to construct a convex polygon shown in Figure 6c.	Internal points satisfying a threshold topological derivative level around the central point from step 2, are used to construct a convex polygon shown in Figure 6c.
5	The vertices of the convex polygon are taken as control points to generate two NURBS curves to insert the new hole, as shown in Figure 6d.	
6	The above steps are repeated until there are no more internal points selected in step 2.	

Table 1: Hole insertion criteria

a bi-directional material approach, i.e. material addition and removal takes place simultaneously during the optimisation iterations, which is equivalent to an evolutionary approach presented in [31]. The boundary element analysis provides σ_V at each node of the structural boundary. Inefficient material,
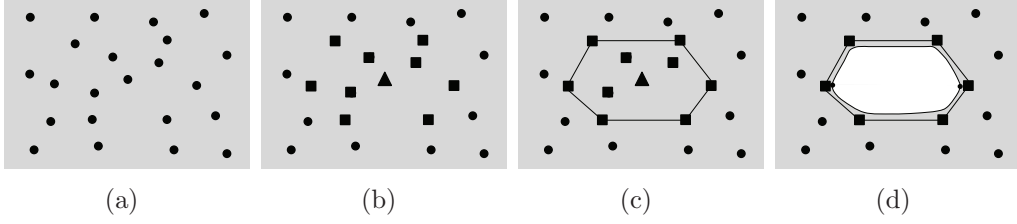
Figure 6: Creation of holes from internal points ($\bullet$ = internal points, $\blacktriangle$ = central internal point, $\blacksquare$ = internal points identified in step 2)

which needs to be progressively removed, is identified as the regions in the locality of nodes satisfying

$$\sigma_V \; < \; RR\,\sigma_{Vmax} \tag{23}$$

where RR is the removal ratio and σ_{Vmax} is the maximum value of σ_V in the initial design. Similarly regions where material should be added are identified as those in the locality of the boundary nodes with high stresses satisfying

$$\sigma_V \; > \; \min(\sigma_{Vmax}, \sigma_Y) \tag{24}$$

where σ_Y is the material's yield stress. The initial removal ratio RR is 0.01, and this is increased periodically as the optimisation progresses by an incremental removal ratio RR_i as,

$$RR = RR + RR_i \tag{25}$$

Each time RR_i is updated, when the combined volume of material experiencing $\sigma_V < RR\,\sigma_{Vmax}$ falls below a threshold of $0.4V$ (where V is the volume at the current iteration), until the stopping criterion is satisfied. The values

22

of RR_i used are discussed in each example in Section 5. Material addition takes place by the outward movement of external boundary and the inward movement of internal boundaries (i.e. holes), while in the material removal process the external boundary is moved inward and the internal boundaries are moved outward.

The structural boundaries are modified during the optimisation process with the LSM, in which the structural boundaries evolve through the velocity function F. In a level set optimisation method the most common approach adopted for the calculation of boundary velocity is based on the shape derivative (e.g., see [3, 4, 8, 10]). As stated in the introduction, gradient based optimisation can be more efficient than the evolutionary methods, although it requires computation of suitably accurate gradients, which may not be available. In the current research work the optimisation method is based on a non-gradient approach, i.e., BESO and the von Mises stress at the boundary nodes is used as a criterion for the advection speed F to evolve the structural geometry. This selection is based on two main reasons. Firstly, Li et al. [ref] suggested that in an ESO method the compliance minimisation problem can be solved by directly using the von Mises stress criterion, and vice versa. Secondly, in a BESO approach (used in this research work) material addition and removal takes place simultaneously. According to Equation (24) the material addition is based on the yield stress which is normally used as failure indicator in structural design. Therefore, it is more appropriate to use the von Mises stress directly instead of the local strain energy. A relationship similar to that proposed by Sethian and Wiegmann [2] has been developed through numerous numerical experiments, and is used to convert

23

σ_V at each node point to the velocity F, as depicted in Figure 7. The intervals shown in Figure 7 can be characterised in terms of σ_V, RR, σ_Y, and σ_{Vmax}, as follows:

- $\sigma_V \in [0, \sigma_{t1}]$ $: \sigma_{t1} = 0.5 \, RR \, \sigma_{Vmax} \, , F = -1$

- $\sigma_V \in [\sigma_{t1}, \sigma_{t2}] : \sigma_{t2} = 0.9 \, RR \, \sigma_{Vmax} \, , F \in [-1, 0]$

- $\sigma_V \in [\sigma_{t2}, \sigma_{t3}] : \sigma_{t3} = 0.95 \min(\sigma_{Vmax}, \sigma_Y) \, , F = 0$

- $\sigma_V \in [\sigma_{t3}, \sigma_{t4}] : \sigma_{t4} = \min(\sigma_{Vmax}, \sigma_Y) \, , F \in [0, 1]$

- $\sigma_V \in [\sigma_{t4}, \infty) : F = 1$

The LSM requires the velocity to be defined at each level set grid point. In this step only the boundary velocity is calculated; the velocity extension method explained in the following section is later used to extend the boundary velocities to the level set grid points.

4.3. Level set implementation

The following procedure is used to integrate the LSM with the optimisation algorithm.

1. The initial structural geometry is embedded as a higher-dimensional function through signed distance calculations, and this initializes the level set grid. Re-initialization of the level set grid is carried out after each hole insertion and during the optimisation process to maintain the level set function as a signed distance.

2. The velocity (calculated in Section 4.2.3, defined at the structural boundary) is only extended to the grid points in the narrow band
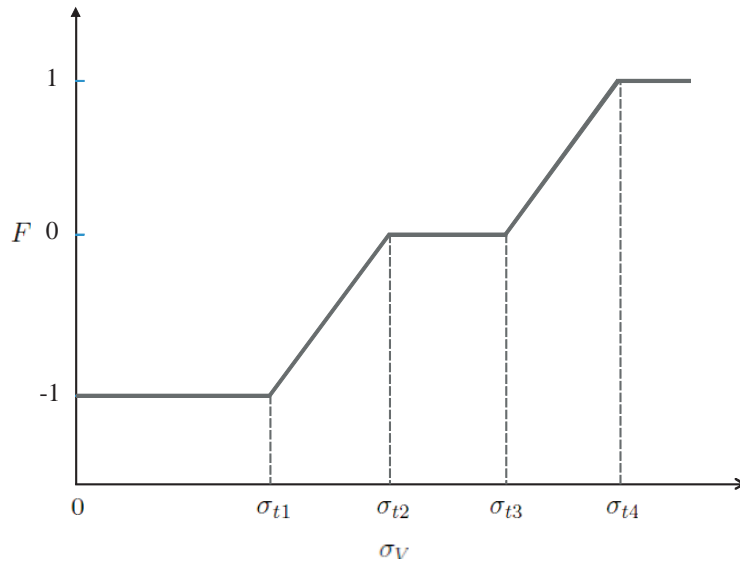
24

Figure 7: Conversion of σ_V to F

around the boundary, using the methods developed by Adalsteinsson and Sethian [32, 33].

3. The solution of (1) with an upwind finite difference approximation update the level set function ϕ.

4. The new zero level set contours are traced with an efficient contour tracing algorithm developed within the CA software. This algorithm linearly interpolates the positions of the zero level set points at the intersections with the level set grid lines.

4.4. NURBS geometry

There are two options available to convert the zero level set intersection points into an updated geometry ready for BE analysis. For explanation purposes a small portion of the level set grid is shown in Figure 8a and the positions of zero level set intersection points are shown in Figure 8b. In the

first option line segments are used to connect the zero level set intersection points (Figure 8c). This yields a non-smooth polygonal structural geometry with line segments of non-uniform length. This geometry is required to be used in structural analysis in the next iteration. In the boundary element analysis if the zero level set intersection points are used directly as element nodal points (as in [25]), two intersection points can lie very close to each other (for example see Figure 8c), and this can cause difficulties and instabilities during the boundary element analysis. In addition the non-smoothness of the polygonal geometry can produce high stress concentrations, which can mislead the optimisation process. In order to overcome these difficulties the curve fitting techniques available in [34] are used to fit a single NURBS passing through the zero level set intersection points (see for example Figure 8d) for each of the modifiable segments of the structural geometry. In this algorithm we use B-splines (a special case of NURBS) to represent the modifiable structural geometry segments. It appears from Figure 3 that the conversion of the boundary from the zero level set to a NURBS representation introduces some approximation, especially at the top and bottom right corners. It can be seen in Figure ?? that the NURBS passes through the zero level set intersection points and therefore, the effect of this approximation die out very quickly in the preceding optimisation iterations as demonstrated in the numerical examples.

The fitted NURBS geometry (Figure 8e) is abstracted from the locations of the level set intersections. The automatic meshing facility in the CA software is used to define elements on each spline, using a setting which is designed to produce peak stresses to approximately 1% accuracy, either

26

(a) Level set grid

(b) Zero level set intersection points

(c) Line segments connecting intersection points

(d) NURBS through intersection points

(e) NURBS
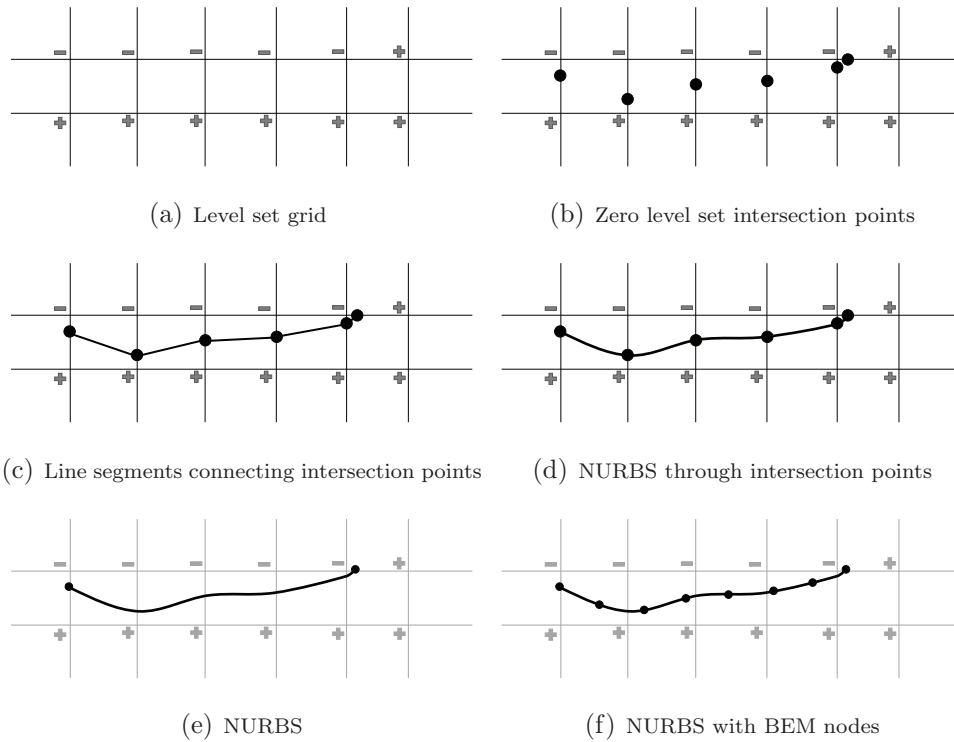
(f) NURBS with BEM nodes

Figure 8: NURBS geometry

with uniformly distributed boundary element nodes as shown in Figure 8f or with grading as required for good BEM meshing practice. A linear elastic stress analysis is then automatically initiated. It should be noted that the boundary-only meshing naturally avoids problems of checkerboarding that are well known to require care in FEM optimisation schemes.

5. Examples

The validity and efficiency of the proposed optimisation method are tested against some benchmarking problems in the field of structural optimisation.

27

The material properties used in these examples are: Poisson's ratio = 0.3, Young's modulus = 210 GPa, Yield stress = 280 MPa. Plane stress conditions are assumed with arbitrary thickness of 1 mm.

5.1. Example-1

The first example is a short cantilever beam with an aspect ratio of 1.0. The geometry of the structure shown in Figure 9, is constrained at the top and bottom of the left edge, and a load of 100 N is applied in the downward direction at the right-hand end of the bottom edge of the beam. The evolutionary parameters used during the optimisation process are $RR = 0.01$ and $RR_i = 0.01$. The optimisation process terminates at the specified volume fraction, i.e. when $\alpha = 0.35$.
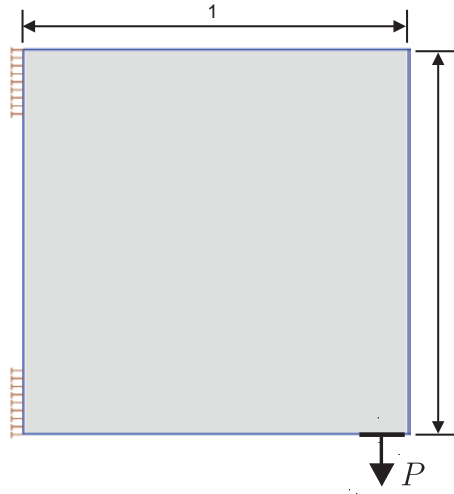
Figure 9: Design domain, loading and boundary conditions for short cantilever beam.

In order to validate the selection of k_V and the correlation between the hole insertion criteria, five different cases are studied in this example. In each

case the values f_V, f_T (used in accordance with (22)) and the corresponding optimisation iterations used to reach the optimal design are shown in Table 2.

Test case	A			B		
	f_V	Total iterations	f_U	f_T	Total iterations	f_U
1	1.3	174	405	1.69	200	432
2	1.4	184	430	1.96	125	412
3	1.5	130	422	2.25	94	417
4	1.6	130	415	2.56	123	430
5	1.8	102	478	3.24	88	427

Table 2: Hole insertion factors and total number of optimisation iterations used in each case of Example 1.

In the first case of this example, the given structure is tested against each of the hole insertion criteria independently and the evolution of structural geometry at various volume fractions is shown in Figure 10. Comparison of results shows that although the size of holes is different, their insertion takes place in similar regions of the structure leading to a very similar final optimum design which closely resembles that commonly presented in the literature for this type of benchmark example. It should be noted that the use of NURBS provides a very smooth geometry throughout the optimisation process without any jagged edges, providing a stable and accurate BE analysis.

In order to further validate the correlation between criterion A and B with different hole insertion factors, the results obtained in case 2, 3 and

	$\alpha = 0.85$	$\alpha = 0.65$	$\alpha = 0.55$	$\alpha = 0.35$
A				
B				
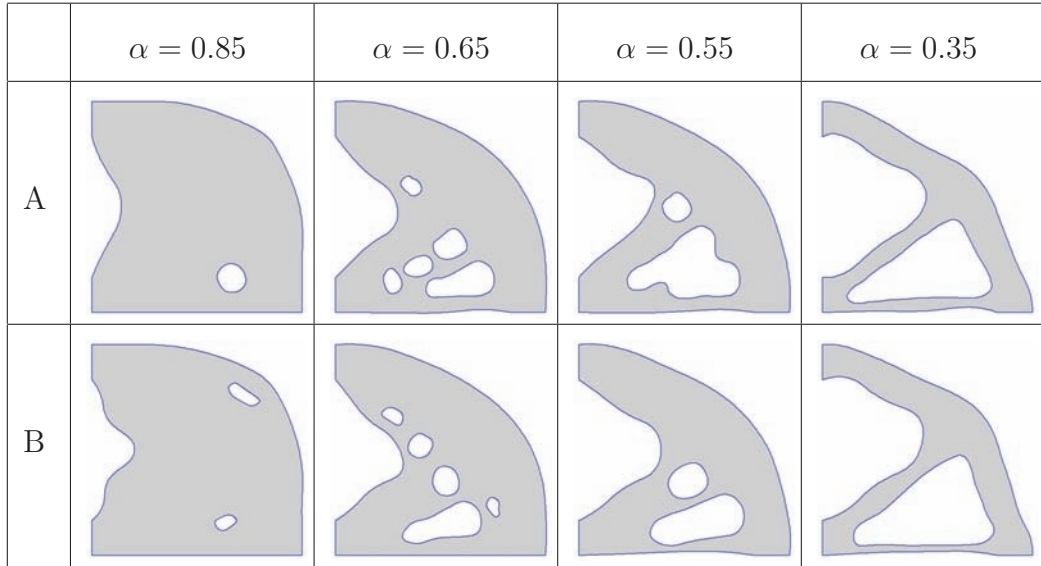
Figure 10: Evolution history of short cantilever beam in Case 1.

4 are presented in Figures 11, 12 and 13, respectively. The results shown in each of these cases indicate a similar behaviour of the evolving and the final optimal geometries, and strongly validate the proposed optimisation method. Furthermore, the results presented clearly demonstrate the correlation between the two criteria as well as the dependency of hole sizes and their insertion rates on the hole insertion factors. It can be seen by the comparison of results in all cases that there are more holes (and also large size holes) with large hole insertion factors at a given volume fraction (e.g. $\alpha = 0.65$), which causes the optimisation process to converge rapidly.

In the last case of this example, the given structure is tested with higher values of the hole insertion factors. The results presented in Figure 14 further validate the dependency of holes sizes on the hole insertion factors, as dis-

	$\alpha = 0.85$	$\alpha = 0.65$	$\alpha = 0.55$	$\alpha = 0.35$
A				
B				
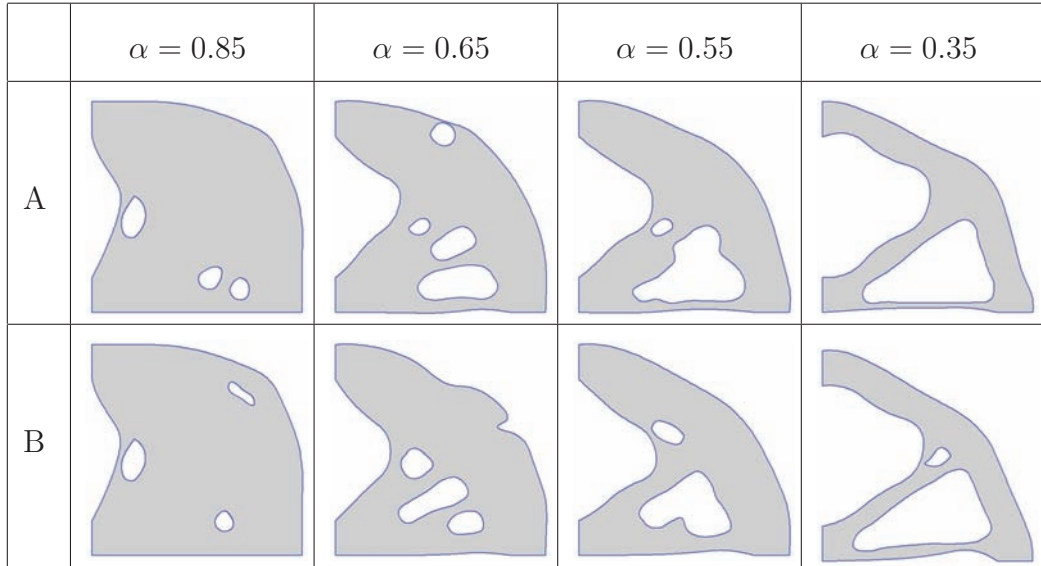
Figure 11: Evolution history of short cantilever beam in Case 2.

cussed in the previous cases. In addition, it is evident from the comparison of case 5 with the previous four cases that, although an increase in hole insertion factors accelerates the optimisation process, at the same time it destabilises the optimisation process leading towards an optimal design which is different from those obtained previously. This suggests that k_V should be used in the range $0.3 \leq k_V \leq 0.6$, but based on the stability and optimum number of optimisation iterations a good choice would be either 0.5 or 0.6.

During the optimisation process the specific strain energy f_U is closely monitored for all the cases and a comparison of the first two cases is shown in Figure 15. The evolution of f_U with respect to the volume fraction for both the cases shows a general reduction with both hole insertion criteria. During the initial iterations in both cases, the hole insertion and boundary
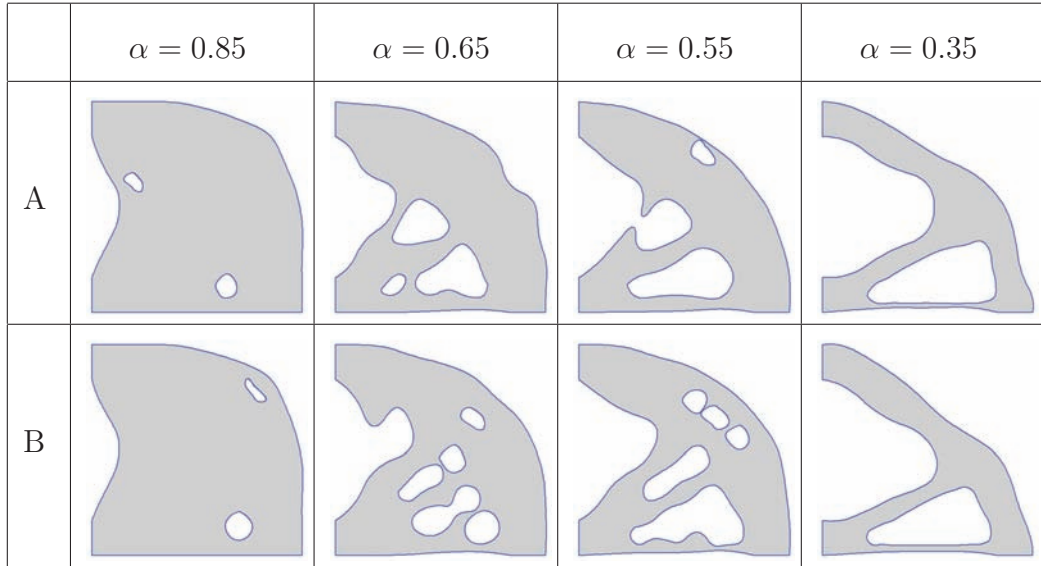
Figure 12: Evolution history of short cantilever beam in Case 3.

movements cause f_U to decrease until α has reduced to 0.60, and then the behaviour starts diverging with some peaks. These peaks are related to the automatic hole insertion and hole merging with the exterior boundary and continue to be observed up to the final volume fraction. The magnitudes of the peaks are large on iterations when a hole is inserted near to the exterior boundary immediately merges with it, but then decay through the optimisation process to reduce f_U. Finally, on termination of the optimisation process when the target volume fraction is achieved, it appears that the specific strain energy is still decreasing, suggesting that extending the optimisation process by more iterations would enable further reduction in this performance indicator if desired. In both of the cases, the optimisation process terminates at different f_U levels with an approximate difference of
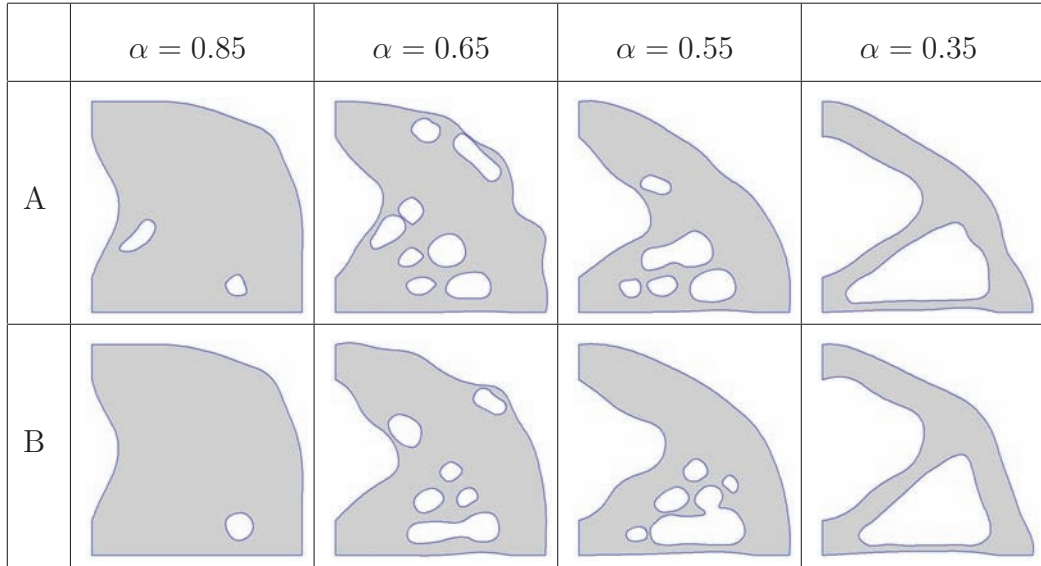
Figure 13: Evolution history of short cantilever beam in Case 4.

6% and 4% in the first and second case, respectively. The difference between f_U in each case with the two criteria is due to different peaks at different stages during their evolution. The randomness in the internal points causes the insertion of holes near the exterior boundary at different locations and with different sizes.

The computational efficiency of the proposed optimisation method is further validated with different initial designs. Foe this purpose three different initial designs have been considered and the optimisation problem is solved using criterion A. The number of holes, f_V, total number of iterations and f_U for each of the case are shown in Table 3. The evolution of structural design in each case is depicted in Figure 16. The optimisation algorithm allows new holes inertion during the optimisation process using the hole insertion

	$\alpha = 0.85$	$\alpha = 0.65$	$\alpha = 0.55$	$\alpha = 0.35$
A				
B				
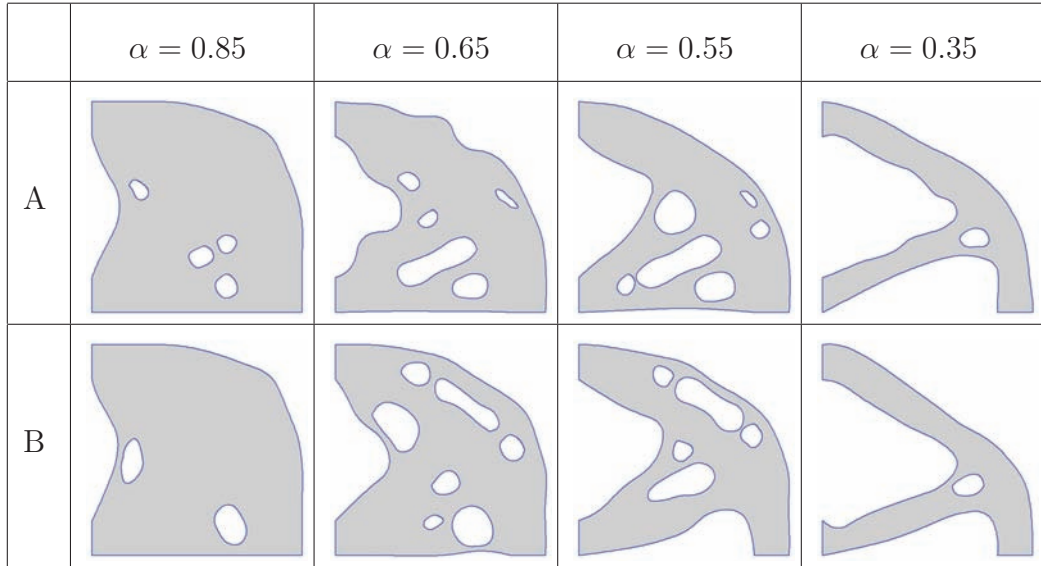
Figure 14: Evolution history of short cantilever beam in Case 5.

criterion. Comparison of results show that for the three different initial designs the final optimal topology obtained are similar to that available in the literature of this type of benchmark example. In addition, the results demonstrate a reduction in the total number of optimisation iterations for the initial design with pre-existing holes with similar performance, i.e., fu.

Initial design	No of holes	f_V	Total iterations	f_U
a	0	1.5	130	422
b	1	1.5	105	420
c	8	1.5	108	416

Table 3: Details of various parameters in the optimisation of different initial designs.

(a) Evolution of f_U with $f_V = 1.3$ and $f_T = 1.69$

(b) Evolution of f_U with $f_V = 1.4$ and $f_T = 1.96$
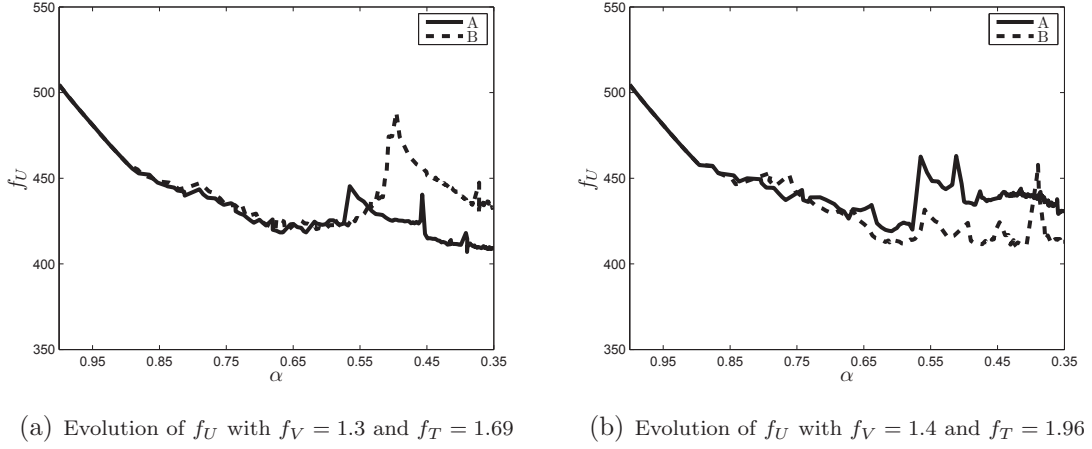
Figure 15: Comparison of the evolution of f_U in Case 1 and 2 of Example 1.

5.2. Example-2

In order to further validate the proposed optimisation method and the correlation between the two criteria, the second example is a cantilever beam with an aspect ratio of 1.6 as shown in Figure 17. The structure is constrained at the top and bottom of the left edge, and a load of 100 N is applied in the downward direction at the middle of the right-hand edge of the beam. In this particular example three different cases are studied in detail. The first two cases demonstrate the correlation between the two hole insertion criteria with a new geometry and constraints, using different hole insertion factors and in the third case a comparison has been made with an increase in RR_i. In all three cases $RR = 0.01$ and the hole insertion factors, total number of optimisation iterations and RR_i used in each case are shown in Table 4. The specified minimum volume fraction for this example is 0.35.

In the first case of this example, the two hole insertion criteria are com-

$\alpha = 1.00$	$\alpha = 0.75$	$\alpha = 0.55$	$\alpha = 0.35$
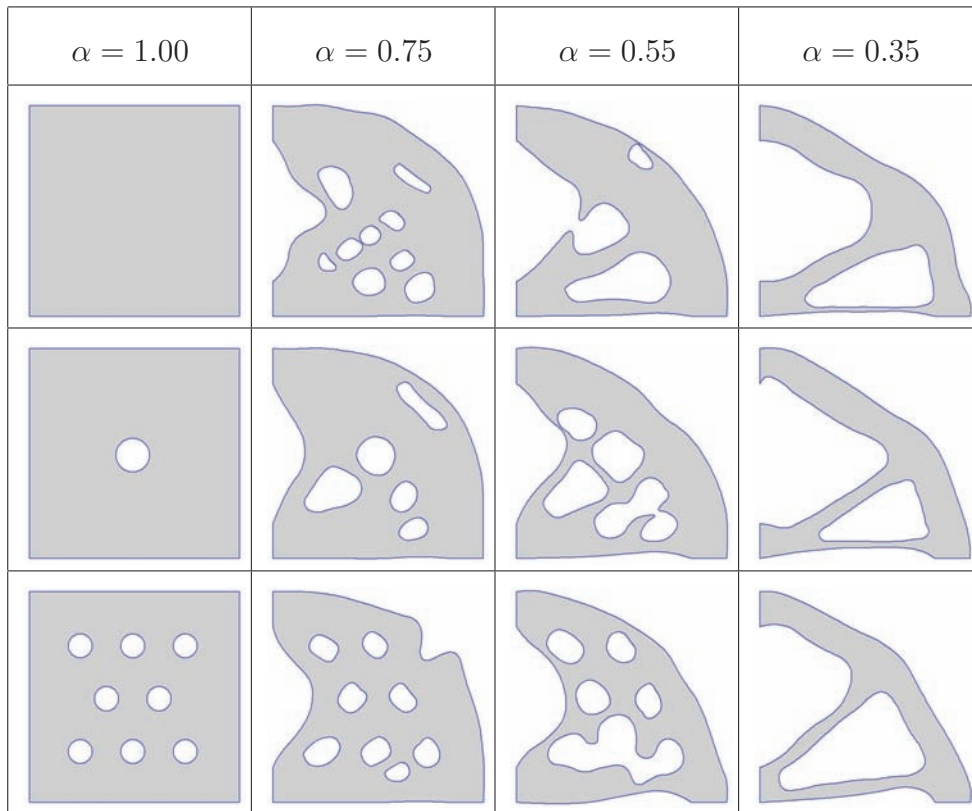
Figure 16: Evolution history of short cantilever beam in Case 3 with different initial designs.

pared in Figure 18. It should be noted that the values of hole insertion factors used are based on the results discussed in the previous example. Comparison of the results shows that holes are inserted in similar regions of the structure with the two different criteria at a given volume fraction (e.g. $\alpha = 0.75$). During the optimisation process the randomness of the internal points causes hole insertions at different locations with criteria A and B, respectively. However, the final optima obtained are very close to each other and also resemble
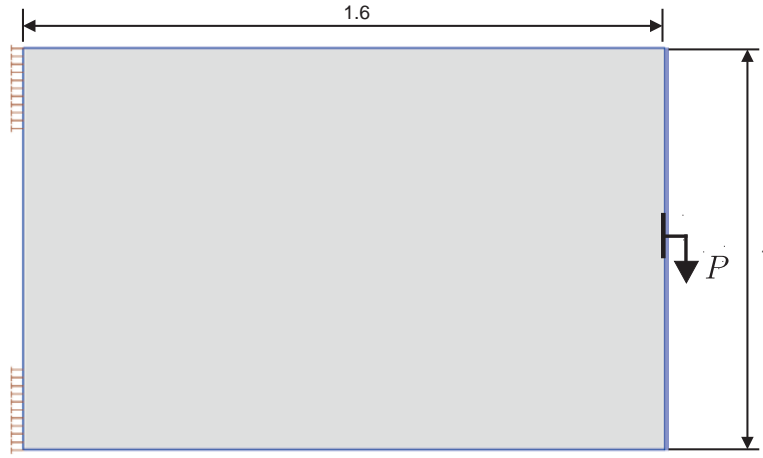
Figure 17: Design domain, loading and boundary conditions for cantilever beam.

Test case	A			B			RR_i
	f_V	Total iterations	f_U	f_T	Total iterations	f_U	
1	1.5	97	1767	2.25	90	1748	0.01
2	1.6	82	1770	2.56	81	1788	0.01
3	1.5	52	1744	2.25	50	1772	0.05

Table 4: Hole insertion factors and total number of optimisation iterations used in each case of Example 2.

the optimal design of this type of benchmark example in the literature. It is evident from the results that an increase in the hole insertion factors gives rise to slightly larger holes in the design domain; this accelerates the optimisation process to converge rapidly to the optimal design as seen in Table 4.

In the third case a comparison has been made with a higher RR_i value.

	$\alpha = 0.75$	$\alpha = 0.55$	$\alpha = 0.35$
A			
B			
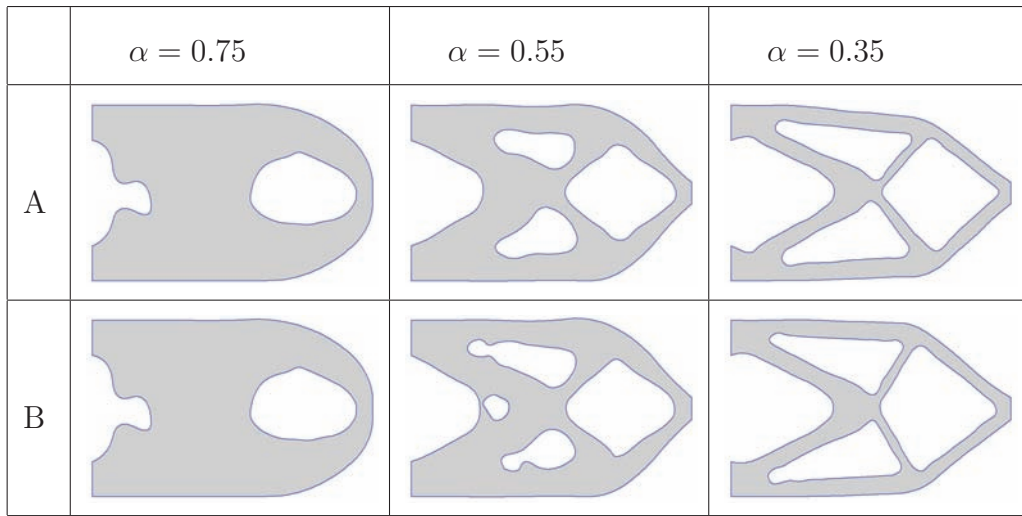
Figure 18: Evolution history of cantilever beam in Case 1.

	$\alpha = 0.75$	$\alpha = 0.55$	$\alpha = 0.35$
A			
B			
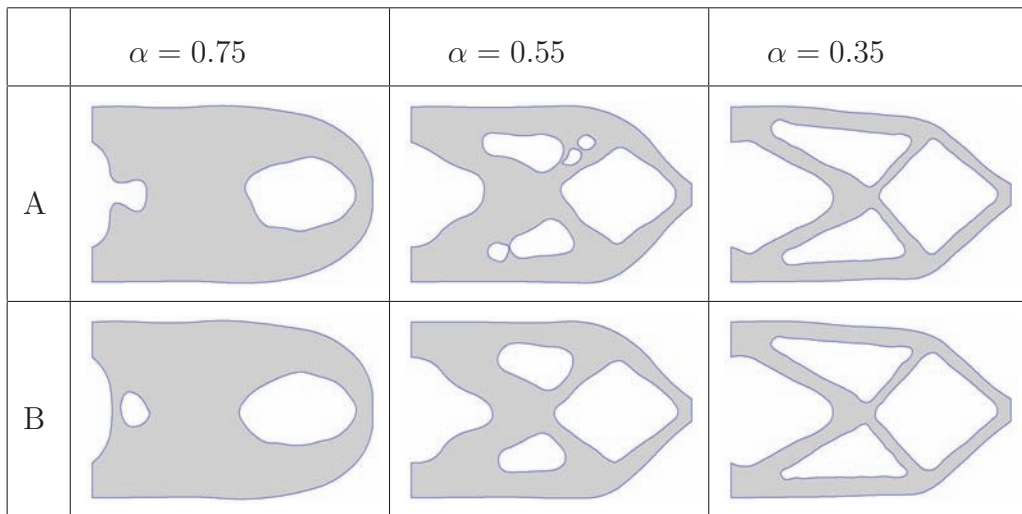
Figure 19: Evolution history of cantilever beam in Case 2.

The results compared in Figure 20 show the same evolution of the optimal geometry as in the previous two cases (i.e. case 1 and 2), but the total number of iterations is considerably reduced (as shown in Table 4). Although Figure 20 shows that for Example 2 the use of $RR_i = 0.05$ can be successful in reducing the required number of iterations, it is recommended to use a lower value of $RR_i = 0.01$. This is because, in some cases a higher value of RR_i causes the removal of an excessive amount of material, destabilizing the optimisation process and leading towards non-converged solutions.

	$\alpha = 0.75$	$\alpha = 0.55$	$\alpha = 0.35$
A			
B			
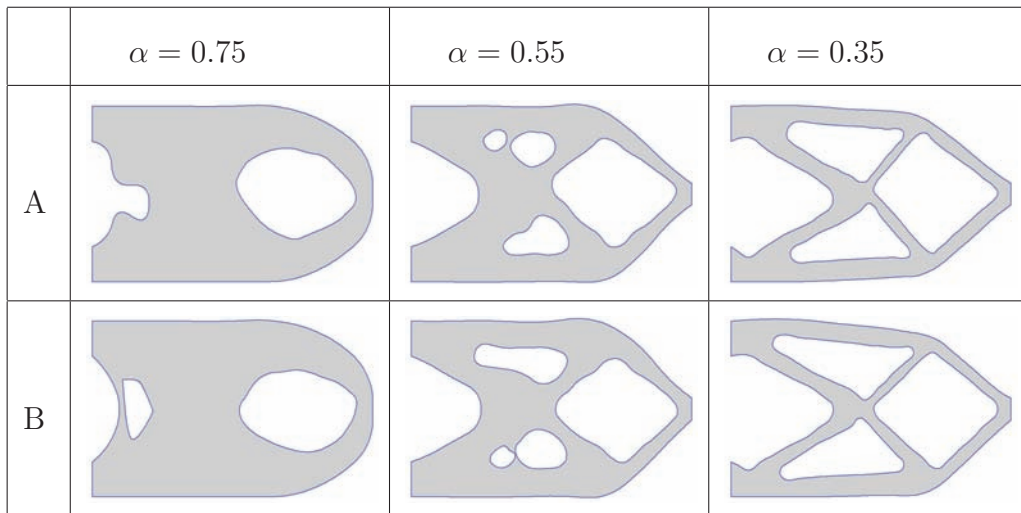
Figure 20: Evolution history of cantilever beam in Case 3.

A similar trend of specific strain energy to the previous example is also observed in this example for the first two cases shown in Figure 21. The peaks occur when a new hole of relatively large size is inserted in the design domain near to $\alpha = 0.75$ and then die out rapidly. It is also evident from this comparison that peaks in Figure 21a are lower than those in 21b. This is due

to the insertion of different size holes with different f_V and f_T in each case. The behaviour of f_U is almost identical up to $\alpha = 0.55$ in both cases with the two criteria; later on the additional hole insertions near the boundary and its immediate merging with it generate high peaks.
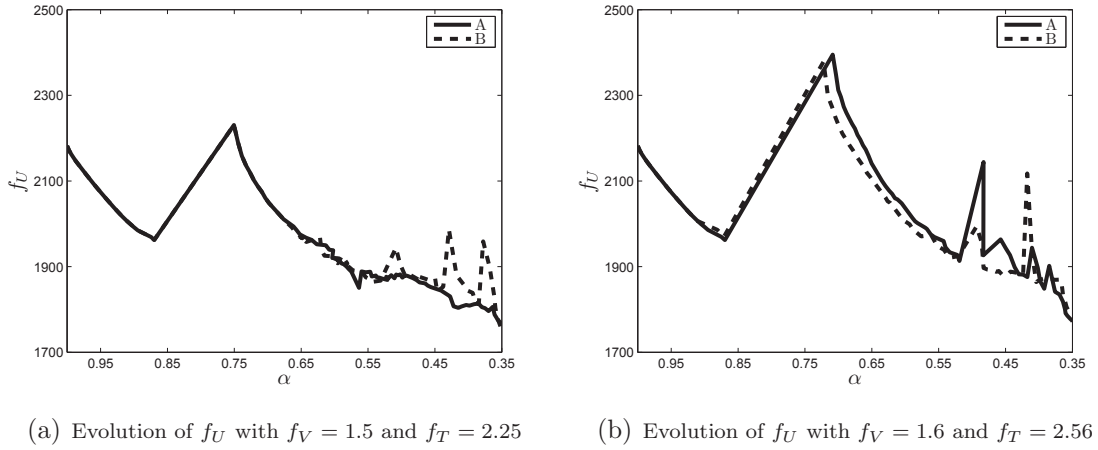

(a) Evolution of f_U with $f_V = 1.5$ and $f_T = 2.25$ (b) Evolution of f_U with $f_V = 1.6$ and $f_T = 2.56$

Figure 21: Comparison of the evolution of f_U in Case 1 and 2 of Example 2.

5.3. Example-3

In this example we apply the proposed optimisation algorithm with different hole insertion criteria to another benchmark example in the field of topology optimisation known as the L-beam [5]. The model is constrained at the top edge and a load of 100 N is applied at the middle of the right edge as shown in Figure 22. The various factors used in this example are: $RR = 0.01$, $RR_i = 0.01$ and the optimisation process terminates when $\alpha = 0.45$.

The results obtained during the optimisation iterations at various volume fractions, α (with the two hole insertion criteria) are depicted in Figure 23.

40
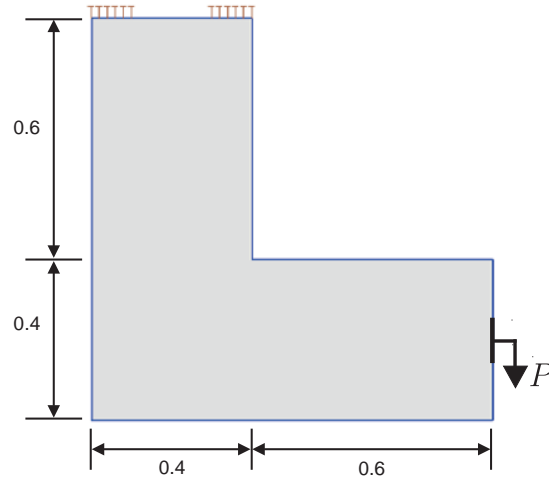
Figure 22: Design domain, loading and boundary conditions for L-beam.

The hole insertion factors used in this example are $f_V = 1.6$ and $f_T = 2.56$. Comparison of the results shows the same behaviour of the evolving geometry as observed in the previous examples. The optimal design generated with the two criteria resembles those available in the literature [5, 35]. The evolution of f_U depicted in Figure 24 with criterion A and B is almost identical and follows the same trend as observed in the previous examples.

In order to validate the capability of the proposed optimisation method for handling the peak stresses, the von Mises stress distribution at different iterations is shown in Figure 25. Comparison of the stress distribution results show that the optimisation method allows the peak stresses, observed at iteration 0, to spread on a smoother surface in the proceeding iterations. This results in an optimal design with a maximum von Mises stress equal to 55. In addition, the use of NURBS automatically smooths the geometry enhancing the convergence towards a smooth optimum.

	$\alpha = 0.75$	$\alpha = 0.65$	$\alpha = 0.55$	$\alpha = 0.45$
A				
B				
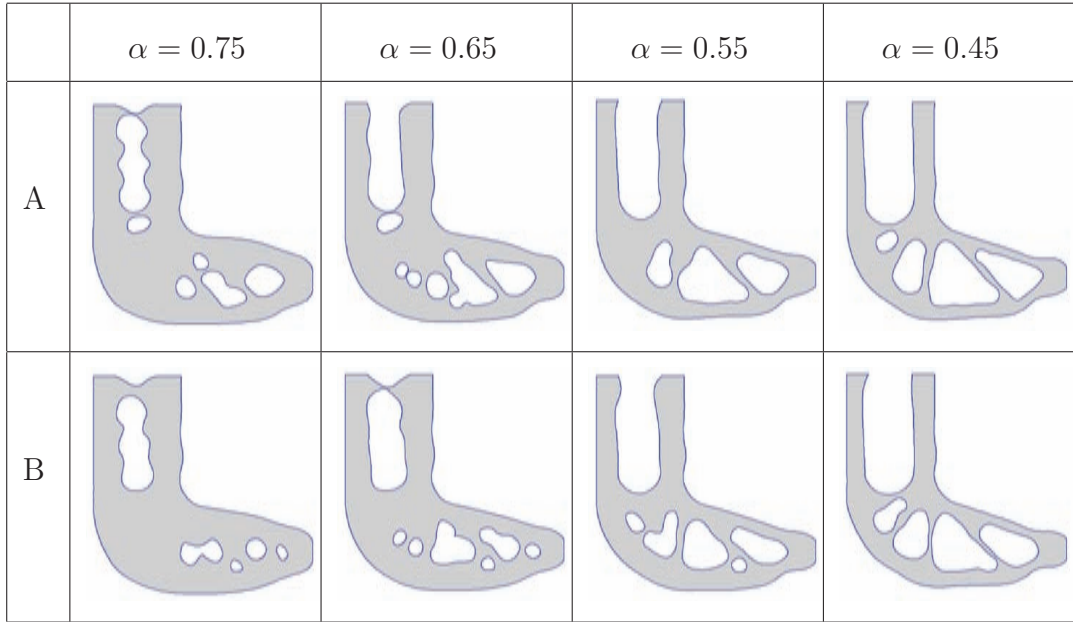
Figure 23: Evolution history of L-beam.

5.4. Example-4

In the final example of this study we apply the proposed optimisation to Michell type structure. The geometry is shown in Figure 26 with an aspect ratio of 1.5 [36, 27]. The structure is constrained around the circular hole in the structure, and a load of 100 N is applied in the downward direction at the middle of the right edge of the beam. The various factors used in this example are: $RR = 0.01$, $RR_i = 0.01$ and the optimisation process terminates when $\alpha = 0.5$.

During the optimisation process the evolution of the structural geometry is depicted in Figure 27 with the two hole insertion criterion, i.e. A and B, respectively. The hole insertion factors used in this example are those used
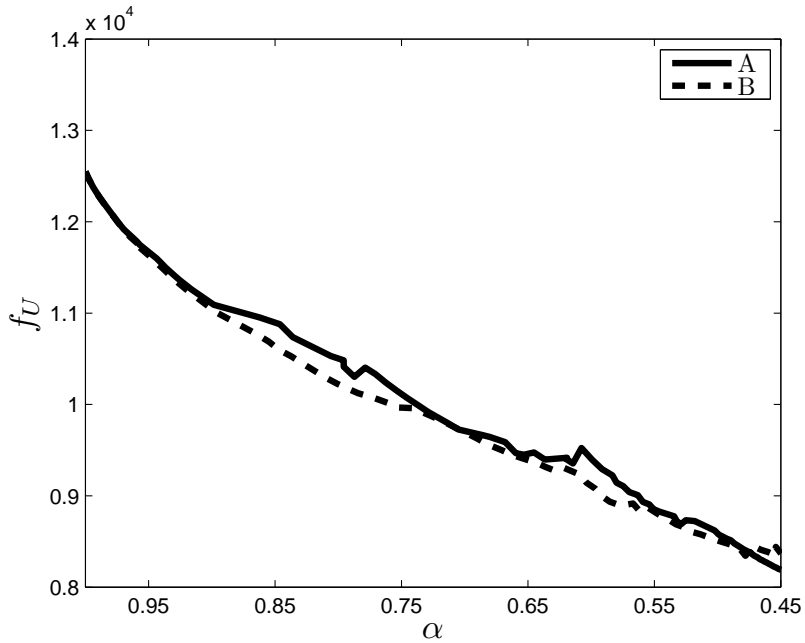
Figure 24: Evolution of f_U for L-beam.

in Example-3. Comparison of the results presented in Figure 27 shows the same behaviour during the optimisation process as observed in the previous examples. The optimal design generated with the two insertion criteria are similar and also very close to those available in the literature [36, 27].

The evolution history of f_U presented in Figure 28 shows similar behaviour to that observed in the previous examples. The evolution of f_U with the two hole insertion criteria are broadly coincident with each other throughout the optimisation process. Up to $\alpha = 0.70$, only boundary movements take place without any hole insertion. The value of f_U drops rapidly when the hole insertion starts in the design domain around $\alpha \approx 0.75$ which is then followed by a slow decrease in f_U until $\alpha = 0.50$ is reached.
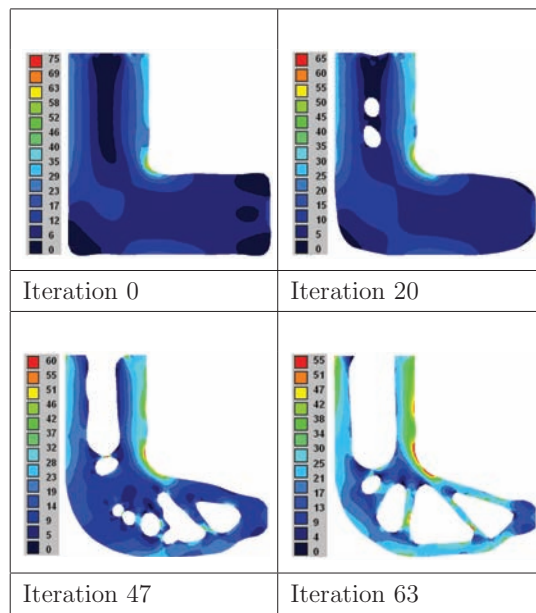
Figure 25: Evolution history of L-beam with von Mises stress contours
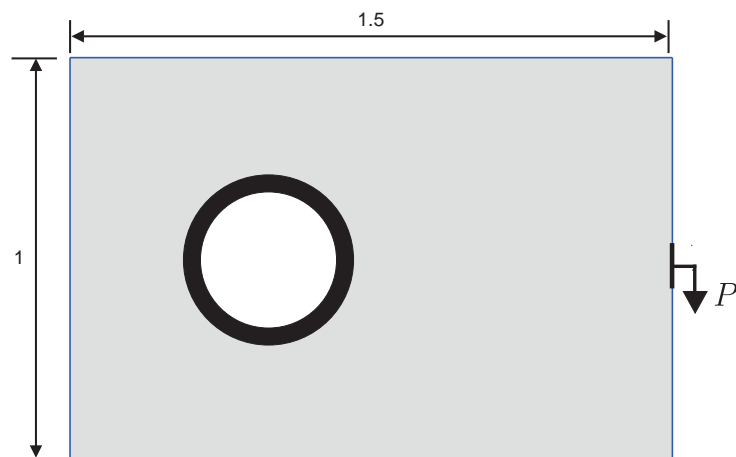
Figure 26: Design domain, loading and boundary conditions for Michell type structure.
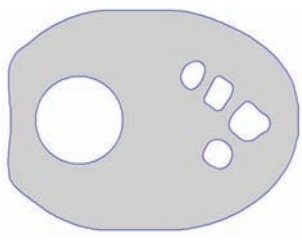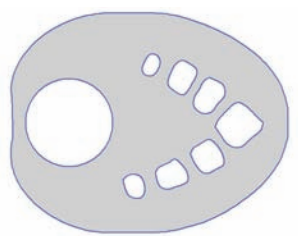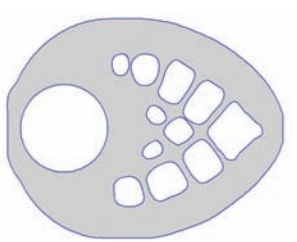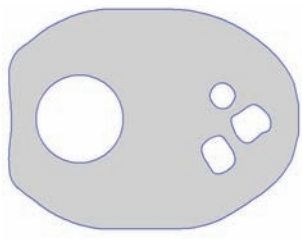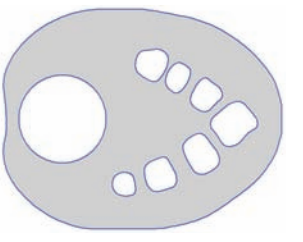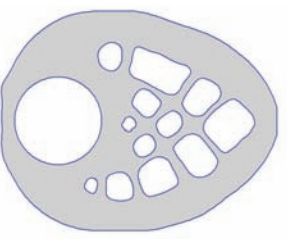
	$\alpha = 0.70$	$\alpha = 0.60$	$\alpha = 0.50$
A			
B			

Figure 27: Evolution history of Michell type structure.

6. Conclusions

In this study, a bi-directional evolutionary structural optimisation approach has been used to study the effect of different hole insertion criteria in a BEM and level set based structural optimisation approach. To the authors' knowledge, the research work presented to date using BEM and LSM based optimisation methods are dependent on initially guessed topologies. In this research work a new optimisation method has been presented for 2D elastic problems which is based on the BEM and LSM. This optimisation method does not rely on an initially guessed topology. Instead two different criteria have been used to automatically insert holes during the optimisation process.

The interesting correlation found between the two hole insertion criteria
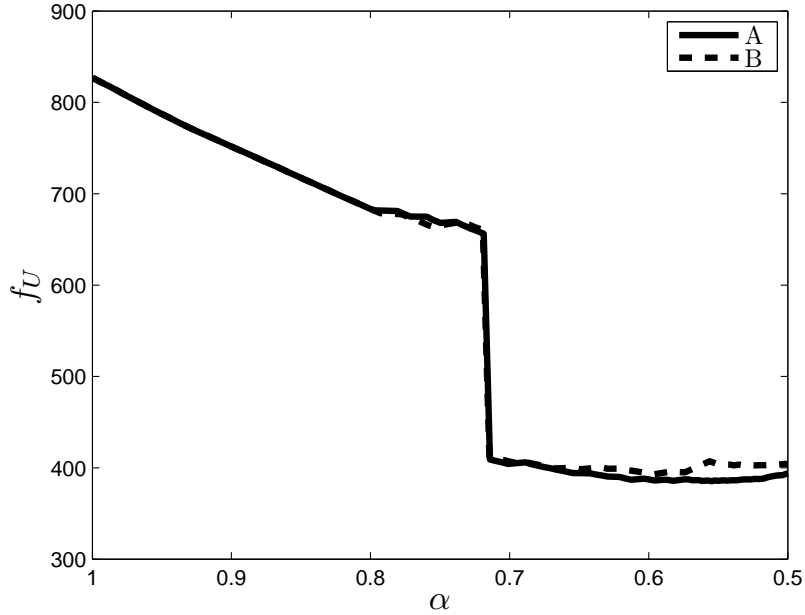
Figure 28: Evolution of f_U for Michell type structure.

has been tested for four different benchmark examples. The results presented for these examples show (i) a close resemblance to optima published in the literature for those cases (ii) the robustness of the proposed optimisation method, and (iii) validation of the correlation between the two hole insertion criteria. This final result is important because it shows that optimisation scheme (proposed in this study, i.e. for stiffness based optimisation problems) driven by simple stress evaluations will produce an optimum that is very strongly correlated, in both geometry and topology, with the optimum determined by schemes based on the calculation of design sensitivities.

In this research work NURBS are used to describe the evolving geometries in a standard CAD format. The use of NURBS completely eliminates

46

jagged edges and checkerboarding which are common problems in FEM based structural optimisation methods.

Acknowledgements

References

[1] S. Osher, J. Sethian, Front propagating with curvature-dependent speed: algorithms based on Hamilton-Jacobi formulations, J Comput Phys 79 (1) (1988) 12–49.

[2] J. Sethian, A. Wiegmann, Structural boundary design via level set and immersed interface methods, J Comput Phys 163 (2) (2000) 489–528.

[3] M. Wang, X. Wang, D. Guo, A level set method for structural topology optimization, Comput Methods Appl Mech Eng 192 (1-2) (2003) 227–246.

[4] G. Allaire, F. Jouve, A. Toader, Structural optimization using sensitivity analysis and a level-set method, J Comput Phys 194 (1) (2004) 363–393.

[5] G. Allaire, F. Jouve, Minimum stress optimal design with the level set method, Eng Anal Bound Elem 32 (11) (2008) 909–918.

[6] T. Yamada, K. Izui, S. Nishiwaki, A. Takezawa, A topology optimization method based on the level set method incorporating a fictitious interface energy, Comput Methods Appl Mech Eng 199 (45-48) (2010) 2876–2891.

[7] H. Jia, H. Beom, Y. Wang, S. Lin, B. Liu, Evolutionary level set method for structural topology optimization, Comput Struct 89 (5-6) (2011) 445–454.

[8] S. Y. Wang, K. M. Lim, B. C. Khoo, M. Y. Wang, An extended level set method for shape and topology optimization, J Comput Phys 221 (1) (2007) 395–421.

[9] J. Luo, Z. Luo, L. Chen, L. Tong, M. Y. Wang, A semi-implicit level set method for structural shape and topology optimization, J Comput Phys 227 (11) (2008) 5561–5581.

[10] P. D. Dunning, H. Alicia Kim, A new hole insertion method for level set based structural topology optimization, Int J Numer Methods Eng 93 (1) (2013) 118–134.

[11] P. Wei, M. Wang, Piecewise constant level set method for structural topology optimization, Int J Numer Methods Eng 78 (4) (2009) 379–402.

[12] G.-W. Jang, Y. Y. Kim, Sensitivity analysis for fixed-grid shape optimization by using oblique boundary curve approximation, International Journal of Solids and Structures 42 (1112) (2005) 3591 – 3609.

[13] S. Wang, M. Y. Wang, A moving superimposed finite element method for structural topology optimization, International Journal for Numerical Methods in Engineering 65 (11) (2006) 1892–1922.

[14] P. Wei, M. Y. Wang, X. Xing, A study on x-fem in continuum structural

optimization using a level set model, Computer-Aided Design 42 (8) (2010) 708 – 719.

[15] S.-H. Ha, S. Cho, Level set based topological shape optimization of geometrically nonlinear structures using unstructured mesh, Computers & Structures 86 (13–14) (2008) 1447–1455.

[16] Z. Liu, J. G. Korvink, Adaptive moving mesh level set method for structure topology optimization, Engineering Optimization 40 (6) (2008) 529–558.

[17] A. Becker, The Boundary Element Methods in Engineering: A complete course, McGRAW - HILL BOOK COMPANY, 1992.

[18] E. Cervera, J. Trevelyan, Evolutionary structural optimisation based on boundary representation of NURBS. Part I: 2D algorithms, Comput Struct 83 (23) (2005) 1902–1916.

[19] E. Cervera, J. Trevelyan, Evolutionary structural optimisation based on boundary representation of NURBS. Part II: 3D algorithms, Comput Struct 83 (23) (2005) 1917–1929.

[20] R. J. Marczak, Topology optimization and boundary elements: A preliminary implementation for linear heat transfer, Eng Anal Bound Elem 31 (9) (2007) 793–802.

[21] A. P. Cisilino, Topology optimization of 2D potential problems using boundary elements, Comput Model Eng Sc 23 (5) (2006) 99–106.

[22] A. Novotny, R. Feijóo, E. Taroco, C. Padra, Topological sensitivity analysis, Comput Methods Appl Mech Eng 192 (7) (2003) 803–829.

[23] L. Carretero Neches, A. Cisilino, Topology optimization of 2D elastic structures using boundary elements, Eng Anal Bound Elem 32 (7) (2008) 533–544.

[24] R. J. Marczak, Optimization of elastic structures using boundary elements and a topological-shape sensivity formulation, Lat Am J Solids Struct 5 (2008) 99–117.

[25] K. Abe, S. Kazama, K. Koro, A boundary element approach for topology optimization problem using the level set method, Commun Numer Methods Eng 23 (5) (2007) 405–416.

[26] S. Yamasaki, T. Yamada, T. Matsumoto, An immersed boundary element method for level-set based topology optimization, Int J Numer Methods Eng (2012) –doi:10.1002/nme.4417.

[27] X. Huang, Y. M. Xie, Evolutionary Topology Optimization of Continuum Structures: Methods and Applications, New York: John Wiley & Sons, 2010.

[28] Q. Li, G. Steven, Y. Xie, On equivalence between stress criterion and stiffness criterion in evolutionary structural optimization, Structural optimization 18 (1) (1999) 67–73.

[29] J. Trevelyan, Concept Analyst. [Online] .www.conceptanalyst.com (2006). [link].
URL `www.conceptanalyst.com`

[30] G. Steven, L. Qing, K. Proos, Y. Xie, The role of physical sensitivity in evolutionary topology design optimisation with multi-criteria and multi-physics, in: P Fifth World Cong Compu Mech (WCCM V). Vienna, Austria., 2002.

[31] O. Querin, G. Steven, Y. Xie, Evolutionary structural optimisation (ESO) using a bidirectional algorithm, Eng Comput: Int J for Comput-Aided Eng 15 (8) (1998) 1031–1048.

[32] D. Adalsteinsson, J. Sethian, The fast construction of extension velocities in level set methods, J Comput Phys 148 (1) (1999) 2–22.

[33] D. Adalsteinsson, J. Sethian, A fast level set method for propagating interfaces, J Comput Phys 118 (2) (1995) 269–277.

[34] D. F. Rogers, An Introduction to NURBS: With Historical Perspective, Morgan Kaufmann, 2001.

[35] Q. Xia, T. Shi, S. Liu, M. Wang, A level set solution to the stress-based structural shape and topology optimization, Comput Struct 90–91 (2012) 55–64.

[36] A. Michell, The limits of economy of material in frame-structures, Phi Mag J Sc 8 (47) (1904) 589–597.